CHAPTER ELEVEN

Use of Small Angle X-ray Scattering (SAXS) to Characterize Conformational States of Functional RNAs[1]

Sebastian Doniach[*,†] *and* Jan Lipfert[‡]

Contents

Abstract

Small-angle X-ray scattering (SAXS) is emerging as an important technique to characterize the structure of RNA molecules. While lower in resolution than X-ray crystallography or NMR spectroscopy, SAXS has the great advantage to have virtually no molecular weight limitations and does not require crystallization. In addition, SAXS can be readily applied under a large range of solution

[*] Department of Applied Physics, Stanford University, Stanford, California, USA
[†] Department of Physics, Stanford University, Stanford, California, USA
[‡] Kavli Institute of Nanoscience, Delft University of Technology, Delft, The Netherlands

[1] Contribution to book edited by D. Herschlag

conditions, allowing to monitor RNA folding, ligand binding, and to characterize partially folded intermediates.

Here, we review how the development of SAXS as a structural technique is driven by advances in computer algorithms that allow to reconstruct low-resolution electron density maps *ab initio* from scattering profiles. In addition, we delineate how these low-resolution models can be used in free energy electrostatics calculations. Finally, we discuss how one can exploit the hierarchical nature of RNA folding by combining the low resolution, global information provided by SAXS with local information on RNA structure, from either experiments or state-of-the-art RNA structure prediction algorithms, to further increase the resolution and quality of models obtained from SAXS.

1. SMALL ANGLE X-RAY SCATTERING (SAXS) AS A TOOL FOR GLOBAL STRUCTURE DETERMINATION AT LOW RESOLUTION

X-ray scattering from molecules in dilute solution is a classic technique dating back to the use of static X-ray tube sources in the 1960s and earlier. However, the relatively low X-ray flux from such sources makes the acquisition of an X-ray scattering profile a matter of hours of exposure. More recently, the use of synchrotron radiation X-rays has made the acquisition of SAXS data much faster, down to a fraction of second exposure time on third generation electron storage ring sources.

When coupled with revolutionary advances in data analysis, whereby a low resolution three-dimensional electron density map may be recovered from the one-dimensional X-ray scattering profile, SAXS has now become a routine technique for characterizing conformational changes in biomolecules (Lipfert and Doniach, 2007; Petoukhov and Svergun, 2007; Putnam *et al.*, 2007). To date such methods have been used to study proteins in solution. Only recently have these methods been applied to the study of RNA molecules in solution (Lipfert *et al.*, 2007a).

2. SAXS AND CONFORMATIONAL CHANGES IN SMALL FUNCTIONAL RNAS

The discovery of catalytic activity in RNA molecules by Cech, Altman, and coworkers in 1982 (Zaug *et al.*, 1983) has led to considerable interest in the structure–function relationships of RNA molecules in biology. Furthermore, it is becoming clear that previously unknown RNA machinery, specified in the noncoding regions of the genome, is essential for controlling expression of genes (Amaral and Mattick, 2008; Mattick, 2007).

As for proteins, X-ray crystallography is the method of choice for determining the structure of RNA molecules when they are in a state that allows for their crystallization. However, even in a folded conformation, RNA molecules present problems for crystallization, partly as a result of their high negative charge.

Changes in conformation involved in the function of RNA molecules often lead to large changes in molecular size and shape and involve only partially folded conformations, which preclude crystallization. In such cases SAXS has proved to be a useful technique which complements more local structural techniques such as FRET, hydroxy radical footprinting, and others, as it gives a measure of the global changes in size and shape of the molecule.

3. SAXS DATA ACQUISITION AND EFFECTS OF RADIATION DAMAGE

An additional practical consideration for measurement of RNA using SAXS is the relatively high scattering contrast of RNA molecules relative to that of proteins as a result of the high density of phosphate moieties in the polynucleotide backbone. This means that shorter exposure times or more dilute samples may be used compared to SAXS measurements for proteins.

In addition, it turns out that RNA is also more resistant to radiation damage than are protein samples, thereby allowing for longer exposure of dilute RNA samples than is possible in the case of protein samples.

A heuristic reason for the extra "radiation hardness" of RNAs turns out to be that the more negatively charged RNA or DNA molecules rather "fall apart" into smaller pieces when hit by X-rays (cf. also the synchrotron footprinting experiments of Mike Brenowitz and coworkers (Sclavi *et al.*, 1998)). As smaller pieces scatter much less, the signal will be influenced less by molecules falling apart. In contrast, damage tends to aggregate proteins. This effect becomes rapidly manifested as the aggregates quickly start to dominate the SAXS signal, due to the $\sim(MW)^2$ dependence of the scattering signal. Detailed protocols and additional practical considerations for SAXS measurements of RNA have been published recently (Lipfert *et al.*, 2009).

4. SAXS DATA ANALYSIS

4.1. Model free analysis

Scattering intensities are isotropic about the direction of the incoming X-ray beam as all molecular orientations are averaged for a dilute solution of molecules. The scattering intensity is obtained from the two-dimensional

CCD data by circular averaging and expressed as a function of scattering angle in terms of the wave vector of momentum transfer q, with $q = 4\pi \sin(\theta)/\lambda$, where 2θ is the total scattering angle and λ the X-ray wavelength.

The scattering profiles may be represented as a plot of $I(q)$ versus q. However, other plots are also useful. An example is the use of the Kratky plot in which $q^2 \times I(q)$ is plotted versus q. This plot is useful on account of Porod's law (Porod, 1951), which states that for large q the scattering from an object with a well-defined surface falls approximately as q^{-4}, which leads to a decrease q^{-2} in the Kratky representation for large q. Folded proteins or nucleic acids therefore tend to have a characteristic peak in the Kratky plot (Kratky and Porod, 1949). For unfolded or random coil polymer states, Kratky and Porod (1949) showed that the scattering from a random polymer falls like $\sim q^{-1}$, which leads to a linear rise at high q in the Kratky plot for completely denatured proteins (Doniach, 2001) or nucleic acids. For RNA molecules in low salt buffer conditions (≤ 200 mM monovalent salt, often referred to as "unfolded" conditions), the Kratky plot typically exhibits a broad and featureless peak at intermediate q values, due to the presence of secondary structure and partial ordering due to electrostatic repulsion. Only upon addition of high concentrations of a denaturant (e.g., 7 M urea) does the RNA completely unfold, giving rise to the typical $\sim q^{-1}$ behavior in the scattering profiles at large q. The onset of RNA folding upon addition of Mg^{2+} to the low salt buffer can typically be monitored by the appearance of a sharper peak, at lower q values than the initial broad peak, in the Kratky plot (Das *et al.*, 2003; Lipfert *et al.*, 2007a, 2008).

The most straightforward application of SAXS is in the determination of the radius of gyration, R_g, of the molecule of interest. This may be estimated from Guinier analysis of the low q data and is a model-free result obtained from the Guinier approximation, valid at low q:

$$I(q) \approx I(0) \exp\left(\frac{-q^2 R_g^2}{3}\right) \qquad (11.1)$$

dependent only on the X-ray wavelength. Here $I(0)$ is the forward scattered intensity and is proportional to the square of the number of electrons in the molecule, relative to the background density of the solvent, and hence scales as the square of the molecular weight. As a result of this q-dependence, the Guinier plot (Guinier, 1939) of the low q region is represented by plotting $\log(I)$ versus q^2. Looking at the slope of this curve gives a practical way of visualizing R_g. This Guinier analysis, which is available numerically in a number of software packages, then also allows for a measure of the molecular weight of the molecule through the extrapolation to $q = 0$. The forward scattering intensity, $I(0)$, may be calibrated by measurements of molecular weight standards, often DNA or proteins samples of known molecular weight and concentration (Lipfert *et al.*, 2009). After calibration of $I(0)$,

Guinier analysis provides a straightforward way to measure the molecular weight of the molecule or molecular complex under study.

The radius of gyration R_g may be expressed in terms of the pair distribution of electron density in the molecule, $P(r)$:

$$R_g = \frac{\int_0^{D_{max}} r^2 P(r)\,dr}{2\int_0^{D_{max}} P(r)\,dr} \tag{11.2}$$

The pair distribution, $P(r)$, and associated maximum atom–atom distance in the molecule, D_{max}, may be estimated via the computer program GNOM (Svergun, 1992). This program performs a regularized indirect transform of the scattering data to obtain $P(r)$, which may be thought of as a histogram of interatomic distances. The $P(r)$ function has a maximum at the most probable intermolecular distance and goes to zero at D_{max}, the maximum intramolecular distance. In order to estimate D_{max}, regularized transforms are performed with the input parameter D_{max} varied in steps of 2 Å. Values of D_{max} are chosen that yielded solutions that (i) fit the experimental data well and (ii) have a smooth and strictly positive $P(r)$ function.

While $P(r)$ provides a useful guide to the general size and internal distribution of electron density in the molecule, it does not give much insight into the three-dimensional form of the molecule, which is not surprising as it only deals with the one-dimensional aspect of the SAXS profile. Nonetheless, it should be noted that the one-dimensional SAXS profiles or, equivalently, the $P(r)$ distributions have the potential to guide *ab initio* structural prediction algorithms which start from the nucleotide sequence (cf. Zheng and Doniach (2002) and Wu *et al.* for the protein case (Wu *et al.*, 2005; Zheng and Doniach, 2002)).

4.2. *Ab initio* three-dimensional shape reconstructions

Although the idea of three-dimensional shape reconstruction from SAXS data dates back to Svergun and Stuhrmann (1991) and Svergun *et al.* (1996), the method became much more practical after the discovery by Chacon *et al.* (1998) that the placement of scattering point "beads," or "dummy atoms," in a spatial array in such a way that the resulting scattering profile fits the experimental data, could lead to low-resolution three-dimensional representations of the electron density in the molecule. This idea was further developed by Walther *et al.* (2000), who tested it out on a variety of protein structures, and by Svergun *et al.* who developed the user friendly programs DAMMIN (Svergun, 1999) and GASBOR (Svergun *et al.*, 2001) which are freely available.

The development of such algorithms which produce candidate three-dimensional electron density maps from one-dimensional scattering profiles has proven extremely useful for understanding changes in conformational size and shape and has let to a boom in the use of SAXS as a structural technique, in particular for proteins and protein complexes. Although the software was developed for protein scattering, it has been subsequently shown by Lipfert et al. (2007b) that it also works for RNA molecules. Test cases with known high-resolution structure from X-ray crystallography include the P4–P6 fragment of the Tetrahymena group I intron ribozyme, tRNA, and short DNA duplexes. The advantage of SAXS for RNA structure determination is that it also may be used for partially unfolded structures for which crystallization is impossible or even in the case of folded states of molecules for which crystallization has not yet become available.

It is important to realize that the reconstruction of a three-dimensional density map from a one-dimensional scattering profile is not unique. Alternative solutions for a given three-dimensional reconstruction cannot in general be avoided, owing to the lack of phase and angular orientation information inherent in SAXS measurements. Such alternative solutions are most prominent for geometrical bodies of high symmetry such as cylinders. However, for real molecules, as shown by Walther et al. (2000), the lack of intrinsic molecular symmetry is generally found to result in a reasonably unique shape reconstruction, usually obtained after averaging over a number of runs of the reconstruction algorithm.

After a number of three-dimensional reconstructions are performed they may be averaged using the program SUPCOMB (Kozin and Svergun, 2001), which performs an initial alignment of structures based on their axes of inertia followed by measurement of their overlap by minimization of the normalized spatial discrepancy (NSD). For two sets of points $S_1 = 1, \ldots, N_1$ and $S_2 = 1, \ldots, N_2$ the NSD is defined as

$$\mathrm{NSD}(S_1, S_2) = \left[\frac{1}{2} \left(\frac{1}{N_1 d_2^2} \sum_{i=1}^{N_1} \rho^2(s_{1,i}, S_2) + \frac{1}{N_2 d_1^2} \sum_{i=1}^{N_2} \rho^2(s_{2,i}, S_1) \right) \right]^{1/2}$$

(11.3)

where $\rho(s_{1,i}, S_2)$ is minimum value among the distances between $s_{i,1}$ and all points from S_2 and d_i is the average distance between neighboring points in S_i.

The NSD has the property that it is zero for identical objects and larger than one for objects that systematically differ from one another (Kozin and Svergun, 2001). The aligned structures can be averaged using the program DAMAVER (Volkov and Svergun, 2002), giving an effective occupancy of
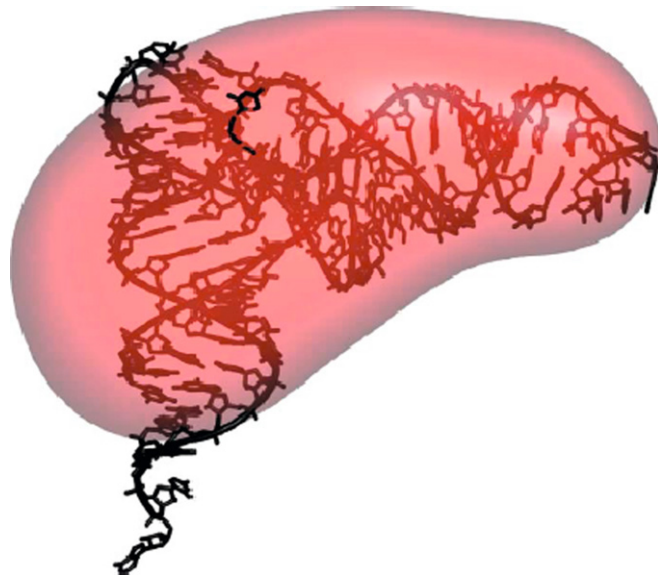
Figure 11.1 Atomic resolution structure of yeast tRNAPhe (PDB accession code 1TRA), rendered as black sticks and reconstructed density (red transparent surface). The reconstructed density was generated from the filtered consensus bead model by smoothing with a Gaussian kernel. Figure adapted from Lipfert *et al.* (2007b).

each voxel. Keeping all occupied voxels generates a convex hull of all models filtering at half maximal occupancy provides ''filtered'' models.

In order to better visualize the results, the reconstructed bead models may be converted to electron density maps using real space convolution with a Gaussian kernel with the program SITUS (Wriggers and Chacon, 2001; Wriggers *et al.*, 1999). An example is shown in Fig. 11.1. A kernel width of 6 Å and voxel spacing of 2 Å were employed. Molecular graphics were prepared using the program PyMOL (DeLano, 2002).

5. LOW-RESOLUTION ATOMIC SCALE MODELS OF RNA: FITTING SECONDARY STRUCTURE RNA MODELS TO THREE-DIMENSIONAL SHAPE MODELS

Although the low resolution density maps obtained from the three-dimensional reconstruction algorithms give insight into the general shape of a molecular conformation, they intrinsically lack information about how the nucleotide sequence fills the space delineated by the map. Progress on solving this problem of fitting the known (or putative) secondary structure

of an RNA molecule into a three-dimensional shape has recently been made by Lipfert *et al.* (2008) for the case of the VS ribozyme, which is the largest of the known nucleolytic ribozymes, and the only one for which there is no crystal structure.

The principle adopted here results from the hierarchical structural organization of RNA molecules (Brion and Westhof, 1997) which generally consist of Watson–Crick double helices joined by junctions which may be two-way, three-way, or four-way (Lilley, 2000). Here, we adopted a global approach in which helical components are assembled as cylindrical bodies into the three-dimensional shape of the molecule.

The three-way helical junctions all play key roles in directing the architecture of the ribozyme. The low-resolution electron density envelope is good enough to fit cylindrical representations of helical segments and has provided a starting point for more detailed structural modeling of the VS ribozyme to include the junctions and tertiary interactions.

The VS ribozyme can be synthesized in either its *cis* or *trans* form. A low-resolution electron density map calculated from SAXS data for the *cis*-acting form of the ribozyme is shown in Fig. 11.2. The map was calculated using the scattering profiles obtained in the presence of 10 mM Mg^{2+}. The electron density maps of the *cis* and *trans* forms reveal extended structures with maximum lengths of 110 and 120 Å, respectively, consistent with the D_{max} values. However, there are some significant differences between the two envelopes. The most obvious difference between the *cis* and *trans*
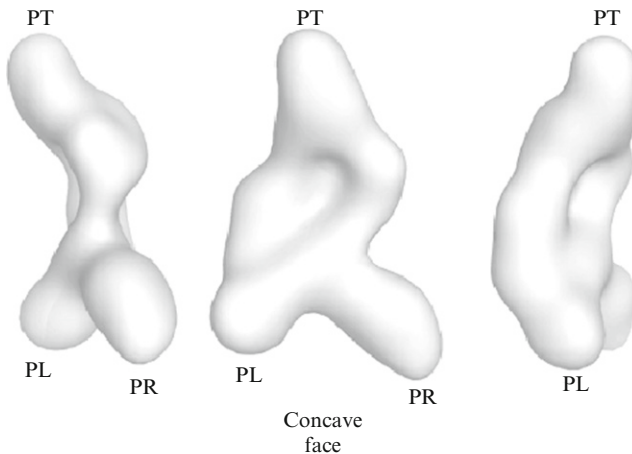

Figure 11.2   Three views of the *cis* VS ribozyme (Lipfert *et al.*, 2008). The central view shows the concave face. The three protuberances extend from the central flat box, labeled PL, PR, and PT. PR is the most prominent. The two side views are shown in the left and right. These clearly reveal the thinness of the envelope.

structures is the presence of a protuberance in the *cis*-ribozyme, strongly suggesting the position of an additional helix. A ridge runs diagonally across the concave face, suggesting the path of a helix.

The irregular envelope of the electron density calculated for the *cis* form of the ribozyme and its subcomponents places considerable limitations on how helices can be fitted, particularly in view of the overall length and a thickness that is close to that of a single helix. A fitting process was performed using cylinders of appropriate length and diameter to represent individual helical sections. In addition, SAXS measurements were made on RNA fragments of the full molecule. Information obtained from fitting to the SAXS data for several of these constructs also helped guide the placement of the helices.

A model of the complete *cis*-acting form of the VS ribozyme was constructed using the cylinder model as a starting point. This exercise was performed to see whether a stereochemically acceptable model based upon the SAXS-derived structure could be constructed that would be consistent with all of the available data. A number of aspects of the structure are presently unknown, and the resulting model should not be confused with an atomic resolution structure. However, it has heuristic value upon which future experiments on the folding and function of the ribozyme may be based. In the final atomic scale model the cylinders with RNA helices were replaced by RNA helices manually located to fit the electron density envelope. In most cases, these were canonical A-form helices and were treated as rigid bodies. Finally, the structure of this model was refined in an iterative manner involving manual adjustment and energy minimization using XPLOR (see Fig. 11.3).

More recently, the use of the RNA structure prediction algorithm MC-SYM (Parisien and Major, 2008) is being used to model the structure of the TPP riboswitch (M. Ali, J. Lipfert, S. Seifert, D. Herschlag, and S. Doniach, in preparation).

6. Determining the Thermodynamics of RNA Folding Using Bead Models

As RNA molecules are highly negatively charged due to their sugar–phosphate backbone, the conformational state of these molecules is strongly dependent on the concentration of positively charged counterions. In the absence of Mg^{2+} or other polyvalent counterions, and in low monovalent salt concentrations, RNA becomes denatured as a result of ineffective Debye screening of the repulsive forces between different parts of the polymer.

As a result, quantitative representation of the counterion induced free energy changes involved in RNA folding and function is of central
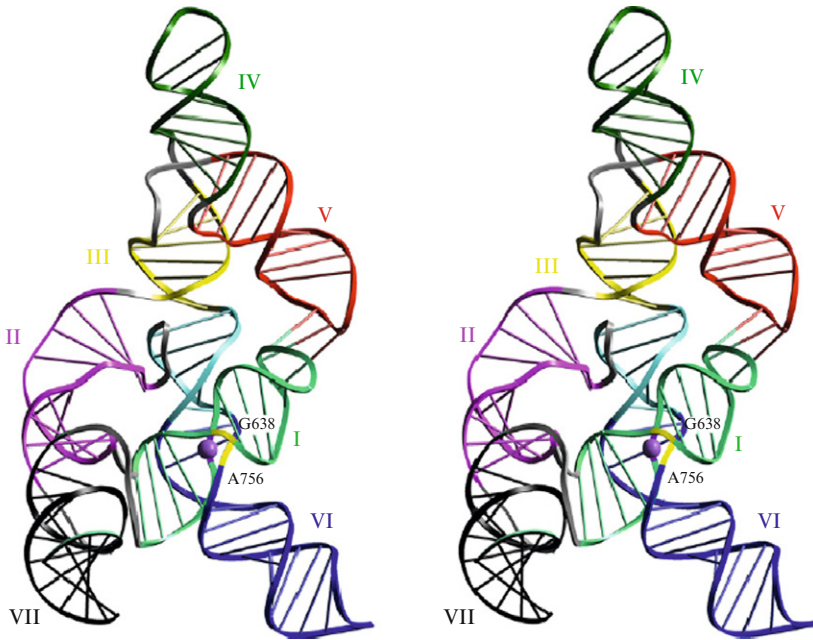
Figure 11.3 Parallel-eye stereoscopic image of a model of the complete VS ribozyme (Lipfert *et al.*, 2008). The model was constructed by connecting previously defined helical sections of a low-resolution model fitting the density map shown in Fig 11.2. Energy-minimization refinement against the standard stereochemical restraints was used to regularize and refine the structure. The scissile phosphate is shown as a sphere, and the probable active site components A756 and G638 are annotated.

importance in understanding RNA folding and the structure–function relationships for RNA molecules. The ability to bind small-molecule ligands or to form protein complexes adds another dimension to this question for certain functional RNAs.

Poisson–Boltzmann theory is widely used to estimate free energy landscapes for counterion induced conformational changes (Chu *et al.*, 2008; Draper, 2008; Draper *et al.*, 2005). Here, one estimates the free energy associated with a cloud of counterions attracted to an RNA (or other charged molecule) by solving self consistently Poisson's equation for the electrostatic potential on a spatial grid embedding the molecule coupled to the Boltzmann factors determining the local concentration of counterions as a function of the electrostatic potential.

To do this (numerically) requires a detailed model of the distribution of fixed charges for the RNA molecule involved. As a consequence, PB analysis has mostly been limited to cases for which high-resolution structures are available from crystallography. However, a complete understanding of

RNA folding requires quantitative models for the free energy of both the folded and *unfolded* conformations, for which no crystal structures can be obtained.

In a recent work by Lipfert *et al.* (2007b), it has been shown that the bead models obtained in three-dimensional reconstruction of the SAXS data can provide a substitute for a detailed atomic model. It was shown that the composition of the associated ions could be adequately calculated using PB theory in combination with SAXS-derived low-resolution bead models. In addition, work in progress suggests that it is possible to use the same strategy to compute the electrostatic contribution to the free energy of RNA folding (J. Lipfert, A. Sim, D. Herschlag, and S. Doniach, in preparation).

To illustrate these ideas we show the results of Lipfert *et al.* on ion binding to the P4–P6 fragment from the Tetrahymena ribozyme (Lipfert *et al.*, 2007b). Das *et al.* (2005) measured the number of bound excess Mg^{2+} ions as a function of $MgCl_2$ concentration in a 2 *M* NaCl background for wild-type P4–P6 and for a mutant that does not bind Mg^{2+} to the "metal ion core." As the two specific "metal ion core" Mg^{2+} binding sites are in the interior of the molecules, our PB calculations (which exclude ions from the interior of the molecule) are not expected to capture their contribution to the overall ion binding. We therefore compare the PB simulations with the ion binding data obtained for the P4–P6 mutant that does not exhibit specific ion binding to the "metal ion core." This approach neglects small, but measurable, differences between the mutant and wild-type P4–P6 solution structures in high salt concentrations (Takamoto *et al.*, 2002). The theoretical predictions using the reconstructed bead model (Fig. 11.4, thick, dashed line) agree reasonably well with the PB calculations for the atomic resolution coordinates (Fig. 11.4, thin, solid line). They slightly under-predict the excess number of Mg^{2+} ions determined experimentally, in particular those obtained using the fluorescence indicator HQS (Fig. 11.4, circles). Overall the agreement with the experiment is remarkable, however, given the fact that the data were obtained in 2 *M* NaCl background and that PB theory is generally expected to be valid only in the low concentration limit.

Once the electrostatic potential, $F(x)$ is known on the grid, the Coulomb contribution of the cloud of counterions to the free energy, ΔG, may be estimated for each new conformation represented by the bead model for partially folded RNAs. However, it should also be mentioned that another important contribution to the total ΔG is the site-specific binding of Mg^{2+} ions. This is a general feature of many crystal structures for folded RNAs. Theoretical estimates of the free energy of specific Mg^{2+} binding would need to take into account possible covalent contributions and so requires very detailed positional information about the bound Mg^{2+} and its binding site environment (mostly oxygen). Thus, it is really only possible for states in which high-resolution crystallographic data is available.
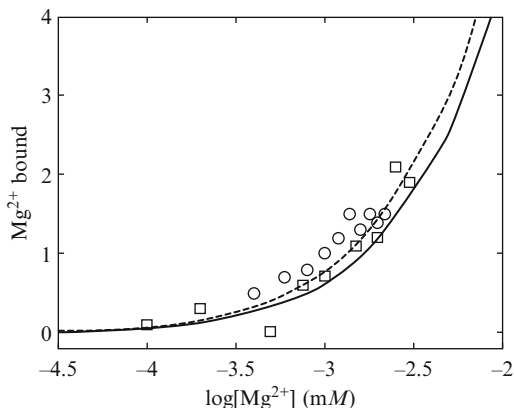
Figure 11.4 Ion binding to a P4–P6 mutant that does not exhibit specific Mg^{2+} binding in the "ion core." The number of excess Mg^{2+} ions was measured using a fluorescence indicator (circles) and atomic emission spectroscopy (squares) by Das *et al.* (2005) in 2 *M* NaCl background. Theoretical predictions were obtained from PB calculations using the PDB coordinates (thin, solid lines) or the reconstructed bead model with uniformly assigned charges (Lipfert *et al.*, 2007b) (thick, dashed lines). Figure adapted from reference Bai *et al.* (2007).

However, as a practical matter, once the counterion cloud contributions have been worked out as discussed above then ΔG values for specific Mg^{2+} binding can be deduced as parameters defining their contributions to thermodynamic models of measured folding curves for the transition between different conformational states of the RNA.

7. CONCLUDING REMARKS

The biophysics of functional RNAs is still at an early stage of development. Many techniques are needed to help relate structure to function for this rapidly growing and highly significant frontier of biology. In particular, *ab initio* structure prediction methods are being developed (Das and Baker, 2007, 2008; Das *et al.*, 2008; Parisien and Major, 2008) that can give reasonable structural models on a local scale. It is at this stage that SAXS, as a global structural technique, is probably the only way available to distinguish predicted structures that provide global structural electron density compatible with the SAXS data. In addition, in the context of structure–function relationships for functional RNA molecules, SAXS measurements contribute in a fundamental way to sorting out some of the needed details of the conformational changes that are central to the function of these molecules.

ACKNOWLEDGMENTS

REFERENCES

Amaral, P. P., and Mattick, J. S. (2008). Noncoding RNA in development. *Mamm. Genome* **19,** 454–492.

Bai, Y., Greenfeld, M., Travers, K. J., Chu, V. B., Lipfert, J., Doniach, S., and Herschlag, D. (2007). Quantitative and comprehensive decomposition of the ion atmosphere around nucleic acids. *J. Am. Chem. Soc.* **129,** 14981–14988.

Brion, P., and Westhof, E. (1997). Hierarchy and dynamics of RNA folding. *Annu. Rev. Biophys. Biomol. Struct.* **26,** 113–137.

Chacon, P., Moran, F., Diaz, J. F., Pantos, E., and Andreu, J. M. (1998). Low-resolution structures of proteins in solution retrieved from X-ray scattering with a genetic algorithm. *Biophys. J.* **74,** 2760–2775.

Chu, V. B., Bai, Y., Lipfert, J., Herschlag, D., and Doniach, S. (2008). A repulsive field: Advances in the electrostatics of the ion atmosphere. *Curr. Opin. Chem. Biol.* **12,** 619–625.

Das, R., and Baker, D. (2007). Automated *de novo* prediction of native-like RNA tertiary structures. *Proc. Natl. Acad. Sci. USA* **104,** 14664–14669.

Das, R., and Baker, D. (2008). Macromolecular modeling with rosetta. *Annu. Rev. Biochem.* **77,** 363–382.

Das, R., Kwok, L. W., Millett, I. S., Bai, Y., Mills, T. T., Jacob, J., Maskel, G. S., Seifert, S., Mochrie, S. G., Thiyagarajan, P., Doniach, S., Pollack, L., *et al.* (2003). The fastest global events in RNA folding: Electrostatic relaxation and tertiary collapse of the Tetrahymena ribozyme. *J. Mol. Biol.* **332,** 311–319.

Das, R., Travers, K. J., Bai, Y., and Herschlag, D. (2005). Determining the Mg^{2+} stoichiometry for folding an RNA metal ion core. *J. Am. Chem. Soc.* **127,** 8272–8273.

Das, R., Kudaravalli, M., Jonikas, M., Laederach, A., Fong, R., Schwans, J. P., Baker, D., Piccirilli, J. A., Altman, R. B., and Herschlag, D. (2008). Structural inference of native and partially folded RNA by high-throughput contact mapping. *Proc. Natl. Acad. Sci. USA* **105,** 4144–4149.

DeLano (2002). http://www.delanoscientific.com

Doniach, S. (2001). Changes in biomolecular conformation seen by small angle X-ray scattering. *Chem. Rev.* **101,** 1763–1778.

Draper, D. E. (2008). RNA folding: Thermodynamic and molecular descriptions of the roles of ions. *Biophys. J.* **95,** 5489–5495.

Draper, D. E., Grilley, D., and Soto, A. M. (2005). Ions and RNA folding. *Annu. Rev. Biophys. Biomol. Struct.* **34,** 221–243.

Guinier, A. (1939). La diffraction des rayons X aux très petits angles: Application à l'étude de phénomènes ultramicroscopiques. *Ann. Phys. (Paris)* **12,** 161–237.

Kozin, M. B., and Svergun, D. I. (2001). Automated matching of high- and low-resolution structural models. *J. Appl. Crystallogr.* **34,** 33–41.

Kratky, O., and Porod, G. (1949). Röntgenuntersuchung gelöster Fadenmoleküle. *Recl. Trav. Chim. Pays Bas* **68,** 1106–1122.

Lilley, D. M. (2000). Structures of helical junctions in nucleic acids. *Q. Rev. Biophys.* **33,** 109–159.

Lipfert, J., and Doniach, S. (2007). Small-angle X-ray scattering from RNA, proteins, and protein complexes. *Annu. Rev. Biophys. Biomol. Struct.* **36,** 307–327.

Lipfert, J., Das, R., Chu, V. B., Kudaravalli, M., Boyd, N., Herschlag, D., and Doniach, S. (2007a). Structural transitions and thermodynamics of a glycine-dependent riboswitch from Vibrio cholerae. *J. Mol. Biol.* **365,** 1393–1406.

Lipfert, J., Chu, V. B., Bai, Y., Herschlag, D., and Doniach, S. (2007b). Low-resolution models for nucleic acids from small-angle X-ray scattering with applications to electrostatic modeling. *J. Appl. Crystallogr.* **40,** S229–S234.

Lipfert, J., Ouellet, J., Norman, D. G., Doniach, S., and Lilley, D. M. (2008). The complete VS ribozyme in solution studied by small-angle X-ray scattering. *Structure* **16,** 1357–1367.

Lipfert, J., Herschlag, D., and Doniach, S. (2009). Riboswitch conformations revealed by small-angle X-ray scattering. *Methods Mol. Biol.* **540,** 141–159.

Mattick, J. S. (2007). A new paradigm for developmental biology. *J. Exp. Biol.* **210,** 1526–1547.

Parisien, M., and Major, F. (2008). The MC-Fold and MC-Sym pipeline infers RNA structure from sequence data. *Nature* **452,** 51–55.

Petoukhov, M. V., and Svergun, D. I. (2007). Analysis of X-ray and neutron scattering from biomacromolecular solutions. *Curr. Opin. Struct. Biol.* **17,** 562–571.

Porod, G. (1951). Die Röntgenkleinwinkelstreuung von dichtgepackten kolloiden systemen. *Kolloid-Zeitschrift & Zeitschrift Fur Polymere* **124,** 83–114.

Putnam, C. D., Hammel, M., Hura, G. L., and Tainer, J. A. (2007). X-ray solution scattering (SAXS) combined with crystallography and computation: Defining accurate macromolecular structures, conformations and assemblies in solution. *Q. Rev. Biophys.* **40,** 191–285.

Sclavi, B., Sullivan, M., Chance, M. R., Brenowitz, M., and Woodson, S. A. (1998). RNA folding at millisecond intervals by synchrotron hydroxyl radical footprinting. *Science* **279,** 1940–1943.

Svergun, D. I. (1992). Determination of the regularization parameter in indirect-transform methods using perceptual criteria. *J. Appl. Crystallogr.* **25,** 495–503.

Svergun, D. I. (1999). Restoring low resolution structure of biological macromolecules from solution scattering using simulated annealing. *Biophys. J.* **76,** 2879–2886.

Svergun, D. I., and Stuhrmann, H. B. (1991). New developments in direct shape determination from small-angle scattering: 1. Theory and model-calculations. *Acta Crystallogr. A* **47,** 736–744.

Svergun, D. I., Volkov, V. V., Kozin, M. B., and Stuhrmann, H. B. (1996). New developments in direct shape determination from small-angle scattering: 2. Uniqueness. *Acta Crystallogr. A* **52,** 419–426.

Svergun, D. I., Petoukhov, M. V., and Koch, M. H. (2001). Determination of domain structure of proteins from X-ray solution scattering. *Biophys. J.* **80,** 2946–2953.

Takamoto, K., He, Q., Morris, S., Chance, M. R., and Brenowitz, M. (2002). Monovalent cations mediate formation of native tertiary structure of the *Tetrahymena thermophila* ribozyme. *Nat. Struct. Biol.* **9,** 928–933.

Volkov, V. V., and Svergun, D. I. (2002). 12th International Conference on Small-Angle Scattering. Venice, Italy.

Walther, D., Cohen, F. E., and Doniach, S. (2000). Reconstruction of low-resolution three-dimensional density maps from one-dimensional small-angle X-ray solution scattering data for biomolecules. *J. Appl. Crystallogr.* **33,** 350–363.

Wriggers, W., and Chacon, P. (2001). Using Situs for the registration of protein structures with low–resolution bead models from X–ray solution scattering. *J. Appl. Crystallogr.* **34,** 773–776.

Wriggers, W., Milligan, R. A., and McCammon, J. A. (1999). Situs: A package for docking crystal structures into low–resolution maps from electron microscopy. *J. Struct. Biol.* **125,** 185–195.

Wu, Y. H., Tian, X., Lu, M. Y., Chen, M. Z., Wang, Q. H., and Ma, J. P. (2005). Folding of small helical proteins assisted by small-angle X-ray scattering profiles. *Structure* **13,** 1587–1597.

Zaug, A. J., Grabowski, P. J., and Cech, T. R. (1983). Autocatalytic cyclization of an excised intervening sequence RNA is a cleavage-ligation reaction. *Nature* **301,** 578–583.

Zheng, W., and Doniach, S. (2002). Protein structure prediction constrained by solution X–ray scattering data and structural homology identification. *J. Mol. Biol.* **316,** 173–187.